Supporting Information: Scanned Single-Electron Probe inside a Silicon Electronic Device

Kevin S. H. Ng,[†,‡] Benoit Voisin,[†] Brett C. Johnson,[¶] Jeffrey C. McCallum,[¶] Joe Salfi,[*,†,§] and Sven Rogge[†]

†*Centre for Quantum Computation and Communication Technology, School of Physics, The University of New South Wales, Sydney, New South Wales 2052, Australia*

‡*5. Physikalisches Institut and Center for Integrated Quantum Science and Technology, Universität Stuttgart, Pfaffenwaldring 57, 70569 Stuttgart, Germany*

¶*Centre for Quantum Computation and Communication Technology, School of Physics, University of Melbourne, Melbourne, Victoria 3010, Australia*

§*Department of Electrical and Computer Engineering, University of British Columbia, Vancouver, BC V6T 1Z4, Canada*

E-mail: jsalfi@ece.ubc.ca

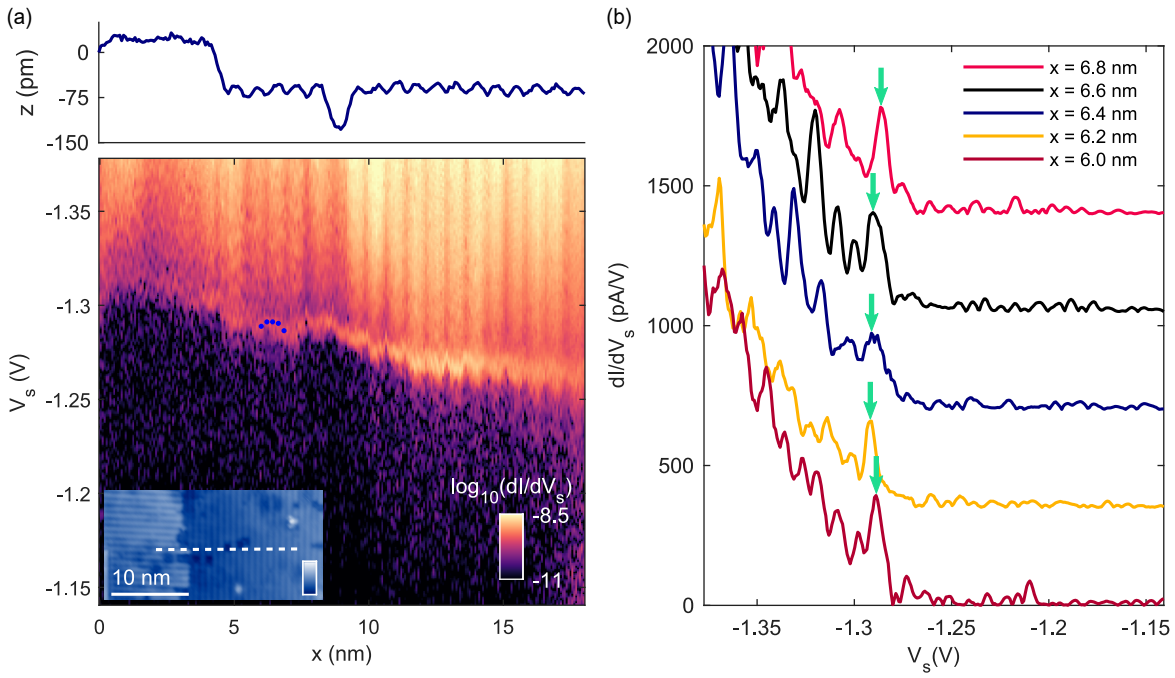

Figure S1: (a) Conductance map of Figure 2a. The position of the dots plotted on the resonance between $x = 6.0 - 6.8$ nm correspond to the traces shown in (b). In this region, there are no surface defects as seen from the plotted topography above. (b) Single conductance traces of the conductance map in (a) between $x = 6.0 - 6.8$ nm. As expected, the position of the resonance peak in V_s, indicated by the green arrows does not shift significantly in this interval. As a result, the peak we attribute to the resonance indicated in Figure 2b for the trace at $x = 6.4$ nm is due to resonant tunnelling through the QD.

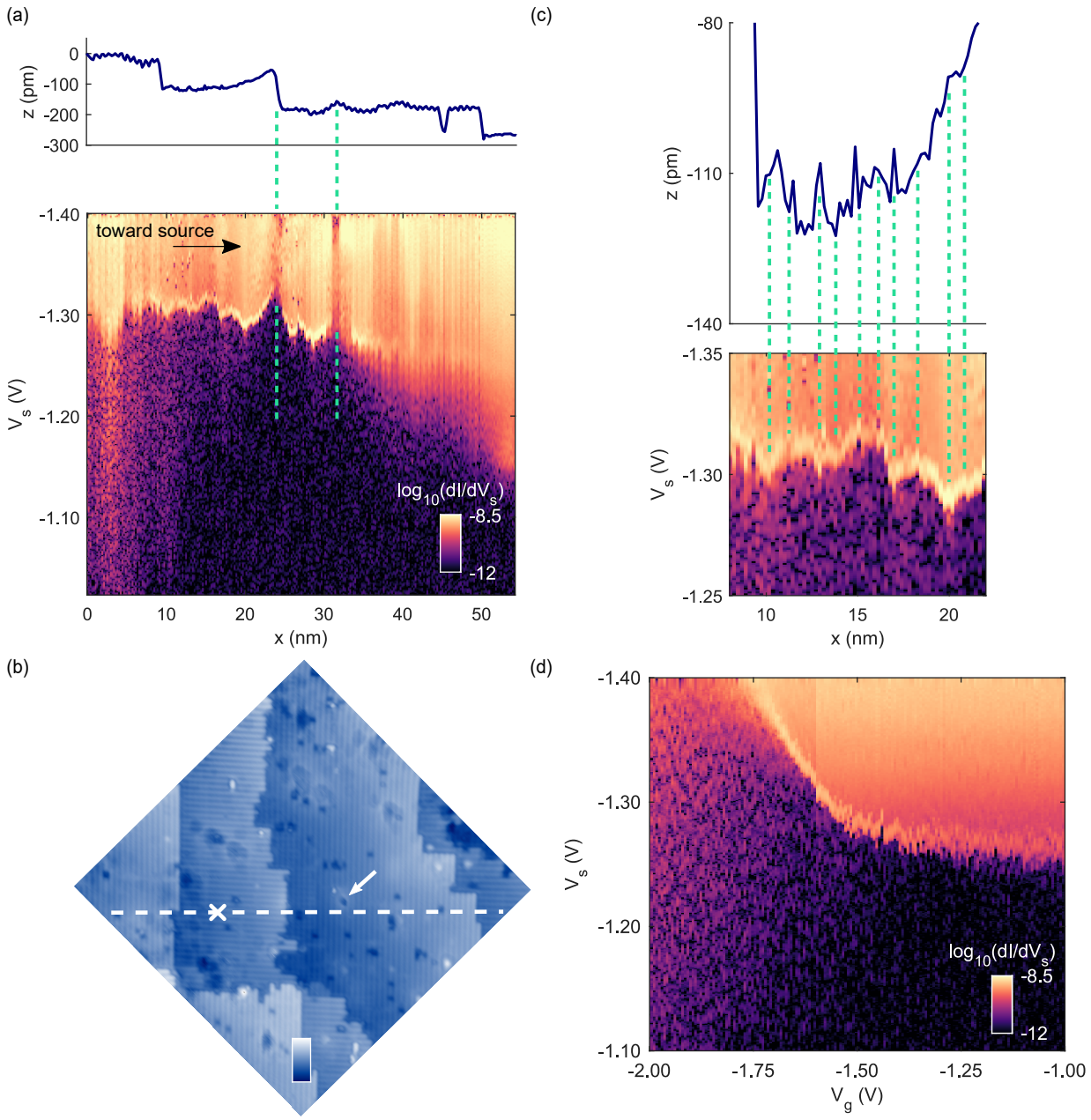

Figure S2: (a) Spectroscopy measurements for a line 58 nm away from Figure 2a. The QD resonance is disturbed by a step edge with accumulated negative charge ($x = 24$ nm) and a negatively charged dangling bond[S1] ($x = 32$ nm) both identified in topography. The dangling bond is momentarily positive when imaged by the tip. As the tip approaches and enters the reservoir, the QD resonance broadens and disappears. Taken at $V_g = -1.6$ V. (b) STM topography taken at $V_s = -1.6$ V, with white line showing where measurement in (a) was taken. The marker on the line indicates the position of the tip during the measurement of (d). The arrow indicates the dangling bond the QD interacts with at $x = 32$ nm. Scale: 0 – 0.36 nm. (c) Close up of the map in (a) and the topography for $x = 8 - 22$ nm. The relatively small disturbances (green lines) cannot be attributed to defects due to lower resolution of the data. (d) Gating characteristics of the resonance taken at the position indicated by the marker on the line of the STM image (b). The same gating behaviour is seen for the QD when compared to Figure 4b.

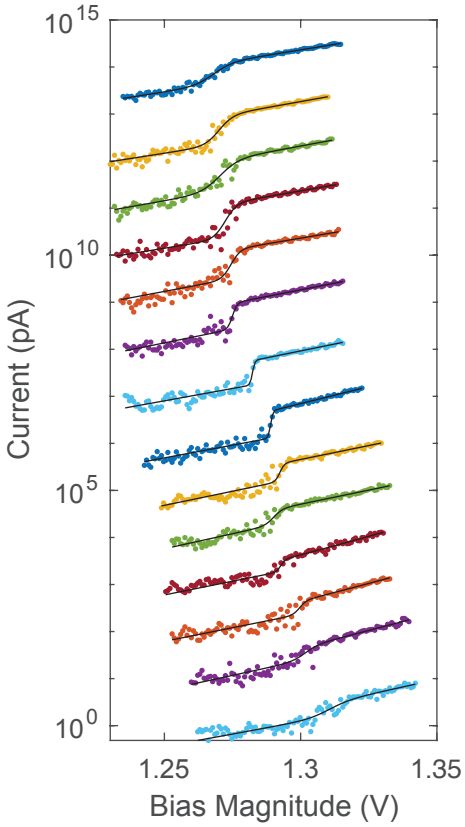

Figure S3: Current traces used to extract ΔI in Figure 3b, taken at the positions of the blue dots plotted on the conductance map of Figure 3a. The traces are plotted with increasing x from bottom to top. The fitting function $I = \Delta I \exp(\Delta_\Gamma(V - V_{thresh}))(1/(1 + \exp(-\alpha_0(V - V_{thresh})/k_B T))) + A\exp(\beta V)$ is used, where ΔI is the step height of the trace at $V = V_{thresh}$, the voltage at which the QD state is on resonance with the source reservoir, Δ_Γ the barrier lowering parameter, α_0 the source-tip lever arm and A and β are parameters of the exponential background current.

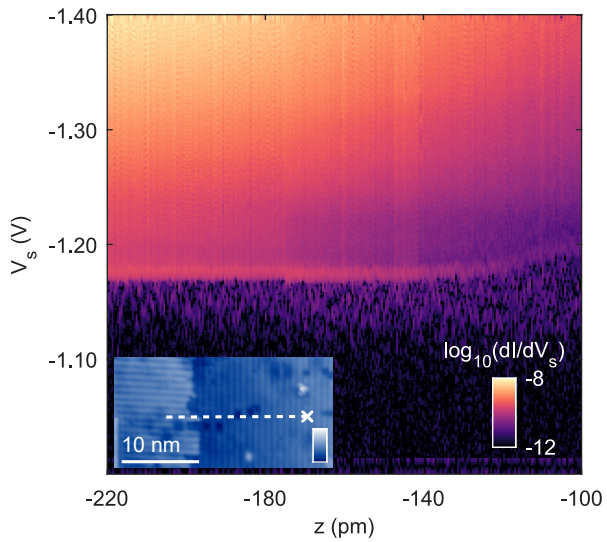

Figure S4: Conductance map during resonant tunnelling as a function of tip height z demonstrating the tunnelling regime $\Gamma_{\text{in}} \ll \Gamma_{\text{out}}$ for all measurements for tip position at the marker in the STM inset at $x = 18$ nm. Γ_{in} here is larger than at $x \approx 4$ nm. No significant change in the conductance peak height and lineshape is observed $\pm$ 20 pm from $z = -200$ pm, the tip height setpoint used for the measurement of Figure 2. As z is increased, the resonance weakens and is eventually not visible as expected. Inset scale: 0 – 0.38 nm.

Quantum dot tunnel coupled to a reservoir

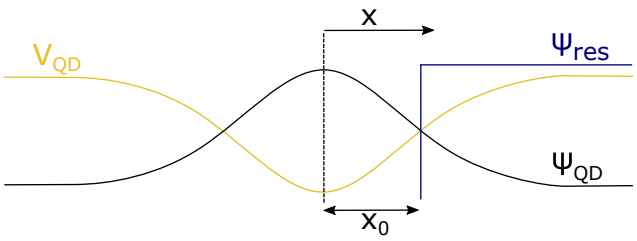

Figure S5: Simplified schematic model of reservoir/QD wavefunction overlap.

Assuming the QD potential V_{QD} is parabolic around the tip ($\sim$ QD centre)[S2] while slowly varying in x and y to 0 far away from the tip, we approximate the tail of ψ_{QD} with an exponentially decaying function $\psi_{QD} = A\exp(-|x|/\lambda)$ and assume the donor reservoir ψ_{res} as homogeneous, normalized to 1 for $x > x_0$, the distance between QD centre and reservoir edge, and 0 otherwise. This is schematically illustrated in Figure S5.

$$
\begin{aligned}
t &= \langle \psi_{QD} | V_{QD} | \psi_{res} \rangle \\
&= AV_{QD} \int_{-\infty}^{\infty} \exp(-|x|/\lambda)\psi_{res} dx \\
&= AV_{QD} \int_{x_0}^{\infty} \exp(-|x|/\lambda) dx \\
&= -AV_{QD}\lambda \left[\exp(-|x|/\lambda)\right]_{x_0}^{\infty} \\
&= AV_{QD}\lambda \exp(-|x_0|/\lambda)
\end{aligned}
$$

$I \sim t^2 \sim \exp(-2|x_0|/\lambda)$ as $\exp(-2|x_0|/\lambda)$ is faster than λ^2. So as the QD approaches the reservoir *i.e.* x increases, x_0 decreases and the current I increases exponentially as measured.

Calculation of the gate lever arm and additional capacitance ratios

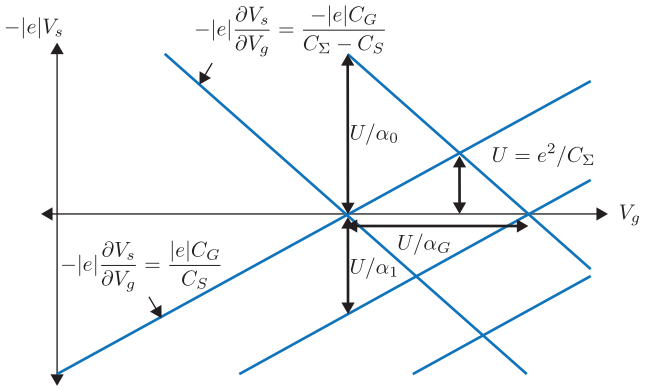

Figure S6: Stability diagram of a single-electron transistor. One of the measured slopes and a measured lever arm parameter are used together to deduce the gate lever arm α_G, which could not be deduced directly from our experiment.

The two measured quantities $\partial V_s/\partial V_g$ and the bias lever arm α_0 can be deduced using only slopes from the Coulomb diagram pattern of the orthodox model for single-electron tunneling. This model is defined in terms of the source capacitance C_S, the gate capacitance C_G, the tip capacitance C_T, and a stray capacitance C_0 (see Figure 4a), and the total QD self-capacitance $C_\Sigma = C_S + C_G + C_T + C_0$, and the stability diagram is shown in Figure S6 from reference[S3].

First, from Figure S6 we can deduce that for $V_S < 0$, the measured parameter $\partial V_s/\partial V_g$ corresponds to $C_G/(C_\Sigma - C_S)$, which was experimentally determined to be 0.77. Second, from Figure S6 we can also deduce that $\alpha_0 = (C_\Sigma - C_S)/C_\Sigma$, which was experimentally determined to be $\alpha_0 \approx 0.1$, and $\alpha_1 = C_S/C_\Sigma$. We can re-write the definition of the gate lever arm $\alpha_G \equiv C_G/C_\Sigma$ in terms of measured quantities α_0 and $\partial V_s/\partial V_g$ as follows:

$$\alpha_G \equiv \frac{C_G}{C_\Sigma} = \frac{C_G}{C_\Sigma - C_S}\frac{C_\Sigma - C_S}{C_\Sigma}$$

which is equivalent to $\alpha_g = \alpha_0 \partial V_s/\partial V_g \approx 0.1 \times 0.77 \approx 0.08$ as discussed in the main text.

Additional capacitance ratios comparing the coupling between the QD and source, gate and tip are calculated (assuming negligible stray capacitance C_0) as follows:

$$\frac{C_G}{C_T} = \frac{C_G/(C_G + C_T)}{1 - C_G/(C_G + C_T)} = \frac{0.77}{1 - 0.77} \approx 3.4$$

$$\frac{C_S}{C_G} = \frac{1 - \alpha_0}{\alpha_0 C_G/(C_G + C_T)} = \frac{1 - 0.1}{0.1 \times 0.77} \approx 12$$

$$\frac{C_S}{C_T} = \frac{C_S}{C_G}\frac{C_G}{C_T} \approx 39$$

References

(S1) Hatem, L.; Marco, T.; Mohammad, R.; Mohammad, K.; Lucian, L.; Jason, P.; Martin, C.; Mark, S.; Robert, A. W. Scanning Tunneling Spectroscopy Reveals a Silicon Dangling Bond Charge State Transition. *New J. Phys.* **2015**, *17*, 073023.

(S2) Dombrowski, R.; Steinebach, C.; Wittneven, C.; Morgenstern, M.; Wiesendanger, R. Tip-Induced Band Bending by Scanning Tunneling Spectroscopy of the States of the Tip-Induced Quantum Dot on InAs(110). *Phys. Rev. B* **1999**, *59*, 8043–8048.

(S3) Hanson, R.; Kouwenhoven, L. P.; Petta, J. R.; Tarucha, S.; Vandersypen, L. M. K. Spins in Few-Electron Quantum Dots. *Rev. Mod. Phys.* **2007**, *79*, 1217–1265.